Received: 27 July 2017 | Revised: 5 February 2018 | Accepted: 10 February 2018

DOI: 10.1002/hbm.24012

RESEARCH ARTICLE

WILEY

Mapping and characterization of positive and negative BOLD responses to visual stimulation in multiple brain regions at 7T

João Jorge[1,2] | Patrícia Figueiredo[1] | Rolf Gruetter[2,3,4] | Wietske van der Zwaag[5,6]

[1]Institute for Systems and Robotics and Department of Bioengineering, Instituto Superior Técnico, Universidade de Lisboa, Lisbon, Portugal

[2]Laboratory for Functional and Metabolic Imaging, École Polytechnique Fédérale de Lausanne, Lausanne, Switzerland

[3]Department of Radiology, University of Lausanne, Lausanne, Switzerland

[4]Department of Radiology, University of Geneva, Geneva, Switzerland

[5]Biomedical Imaging Research Center, École Polytechnique Fédérale de Lausanne, Lausanne, Switzerland

[6]Spinoza Institute for Neuroimaging, Royal Netherlands Academy for Arts and Sciences, Amsterdam, The Netherlands

Correspondence
João Jorge, Laboratory for Functional and Metabolic Imaging, LIFMET-CIBM, Station 6, École Polytechnique Fédérale de Lausanne, CH-1015, Lausanne, Switzerland.
Email: joao.jorge@epfl.ch

Funding information
Centre d'Imagerie BioMédicale (CIBM) of the UNIL, UNIGE, HUG, CHUV, EPFL; Leenaards and Jeantet Foundations; Swiss National Science Foundation, Grant Numbers: 31003A-153070; Portuguese Science Foundation (FCT), Grant Numbers: SFRH/BD/51449/2011, PTDC/EEI-ELC/3246/2012, and PEst-OE/EEI/LA0009/2013

Abstract

External stimuli and tasks often elicit negative BOLD responses in various brain regions, and growing experimental evidence supports that these phenomena are functionally meaningful. In this work, the high sensitivity available at 7T was explored to map and characterize both positive (PBRs) and negative BOLD responses (NBRs) to visual checkerboard stimulation, occurring in various brain regions within and beyond the visual cortex. Recently-proposed accelerated fMRI techniques were employed for data acquisition, and procedures for exclusion of large draining vein contributions, together with ICA-assisted denoising, were included in the analysis to improve response estimation. Besides the visual cortex, significant PBRs were found in the lateral geniculate nucleus and superior colliculus, as well as the pre-central sulcus; in these regions, response durations increased monotonically with stimulus duration, in tight covariation with the visual PBR duration. Significant NBRs were found in the visual cortex, auditory cortex, default-mode network (DMN) and superior parietal lobule; NBR durations also tended to increase with stimulus duration, but were significantly less sustained than the visual PBR, especially for the DMN and superior parietal lobule. Responses in visual and auditory cortex were further studied for checkerboard contrast dependence, and their amplitudes were found to increase monotonically with contrast, linearly correlated with the visual PBR amplitude. Overall, these findings suggest the presence of dynamic neuronal interactions across multiple brain regions, sensitive to stimulus intensity and duration, and demonstrate the richness of information obtainable when jointly mapping positive and negative BOLD responses at a whole-brain scale, with ultra-high field fMRI.

KEYWORDS
draining veins, fMRI, ICA denoising, multisensory, negative BOLD, visual stimulation

1 | INTRODUCTION

Since the discovery of the blood oxygenation level-dependent (BOLD) contrast, functional magnetic resonance imaging (fMRI) has been widely used for in vivo neuroscience. The BOLD contrast is sensitive to the local concentration of deoxyhemoglobin, which in the brain varies according to changes in cerebral blood flow (CBF), cerebral blood volume (CBV), and the cerebral metabolic rate of oxygen ($CMRO_2$). The coupling mechanisms linking neuronal activity with vascular and metabolic processes are still a topic of intense research and debate (Hillman, 2014). Nevertheless, it is generally accepted that a local increase in neuronal activity will raise $CMRO_2$, but also typically induce a strong increase in CBF, resulting in a net positive BOLD response (PBR).

While positive responses to a stimulation paradigm or task are the most commonly studied, sustained paradigm-locked BOLD signal decreases are also often found in various brain regions, and have captured considerable interest (Lauritzen, Mathiesen, Schaefer, & Thomsen, 2012). This effect, termed negative BOLD response (NBR),

Host institution: This study was fully conducted at the Laboratory for Functional and Metabolic Imaging, École Polytechnique Fédérale de Lausanne, Lausanne, Switzerland.

has been robustly observed in humans during, for example, visual stimulation (Shmuel et al., 2002; Smith, Williams, & Singh, 2004), tactile stimulation (Hlushchuk & Hari, 2006; Kastrup et al., 2008; Klingner, Hasler, Brodoehl, & Witte, 2010) and motor tasks (Hamzei et al., 2002; Stefanovic, Warnking, & Pike, 2004). Cortical areas exhibiting NBRs are often found in close proximity to positively-responding regions (Shmuel et al., 2002), or symmetrically in the opposite hemisphere, such as in somatosensory stimulation or motor tasks (Hlushchuk & Hari, 2006; Mullinger, Mayhew, Bagshaw, Bowtell, & Francis, 2014). NBRs have also been reported in cortical regions not directly related to the stimulus modality (Gonzalez-Castillo et al., 2015), such as in auditory areas during visual stimulation, and vice-versa (Laurienti et al., 2002), and also in regions coinciding with the default-mode network (DMN) (Mayer, Roebroeck, Maurer, & Linden, 2010; van der Zwaag, Marques, Hergt, & Gruetter, 2009b).

Due to the complex nature of the BOLD contrast, NBR interpretation has motivated intense debate, with possible underlying mechanisms including local neuronal "deactivation" (decreases in excitatory activity and/or increases in inhibitory activity), passive hemodynamic effects ("vascular steal" from activated nearby regions), or combinations of both (Mullinger et al., 2014; Wade, 2002). Fractional changes in cerebrospinal fluid (CSF) volume, creating fluctuations anti-correlated to grey matter BOLD responses, are also thought to underlie NBRs that can often be observed in certain brain areas bordering CSF compartments (Bianciardi, Fukunaga, van Gelderen, de Zwart, & Duyn, 2011; Bright, Bianciardi, de Zwart, Murphy, & Duyn, 2014; Thomas, Liu, Park, van Osch, & Lu, 2014). While a number of studies have identified vascular steal effects or suggested the existence of central mechanisms for CBF regulation, competing with local demands (Smith et al., 2004; Vafaee & Gjedde, 2004), considerable evidence suggests a dominant influence of local neuronal activity in the generation of cortical NBRs. Negative responses have been found strongly coupled to decreased $CMRO_2$ in the visual cortex (Pasley, Inglis, & Freeman, 2007; Shmuel et al., 2002), primary motor cortex (Stefanovic et al., 2004) and DMN (Lin, Hasson, Jovicich, & Robinson, 2011), and with psychophysiological measures of functional inhibition in somatosensory (Kastrup et al., 2008) and motor studies (Hamzei et al., 2002). Studies combining fMRI with local electrophysiology measures have provided direct evidence of neuronal deactivation, including local field potential and spiking decreases in primate visual cortex (Shmuel, Augath, Oeltermann, & Logothetis, 2006) and rat somatosensory cortex (Boorman et al., 2010). Furthermore, NBR amplitudes in the visual cortex, auditory cortex and DMN have been found to correlate with pre-stimulus alpha-band EEG power (Mayhew, Ostwald, Porcaro, & Bagshaw, 2013), and sensorimotor NBRs have been related to increased mu-band power and evoked potential amplitudes (Mullinger et al., 2014).

The association of NBRs with local neuronal deactivation, even without fully excluding hemodynamic contributions, is an important landmark for fMRI. Under visual stimulation, results from large single-subject datasets have unveiled widespread sustained NBRs in more than 50% of all grey matter (Gonzalez-Castillo et al., 2015). With both positive and negative BOLD responses demonstrating functional significance, their joint characterization is likely to yield richer descriptions of the neuronal interactions occurring in the brain. Relevant insights include not only response localization, but also their temporal dynamics and stimulus dependence. For instance, studies using visual stimuli of varying intensity and duration have reported a tight covariation between PBRs and NBRs in the visual cortex, for both amplitude and temporal profile (Shmuel et al., 2002). In the somatosensory cortex, ipsilateral NBRs to median nerve stimulation were also found to intensify monotonically with stimulus strength (Klingner et al., 2010). However, ipsilateral NBRs to prolonged (20 s) tactile stimulation have been shown to decay faster than contralateral PBRs (Hlushchuk & Hari, 2006), and NBRs to median nerve stimulation revealed relevant differences in onset and peak timing relative to the PBR (Klingner et al., 2011). Because these observations were made for NBRs and PBRs occurring in distinct brain regions, the observed temporal differences could also be partially caused by region-specific differences in hemodynamic coupling or in the BOLD response habituation, not necessarily specific to the type of response (positive or negative). Nevertheless, in the former study (Hlushchuk & Hari, 2006), somatosensory NBRs to ipsilateral hand stimulation were also found to return to baseline substantially earlier than PBRs to contralateral stimulation occurring in the same brain region, and this was observed in either hemisphere. Therefore, these observations may effectively reflect underlying differences in the temporal dynamics of neuronal activations and deactivations, or differences in hemodynamic coupling that may have a response-specific contribution (Mullinger et al., 2014), which become more evident with prolonged stimulation.

While numerous questions remain to be investigated, the study of BOLD responses, particularly negative, is often limited by their typically low amplitude, which can compromise response detection and characterization. The pursuit of stronger magnetic fields for fMRI, offering large gains in functional sensitivity (van der Zwaag et al., 2009a), offers a promising route to mitigate this limitation. As an additional benefit, the shorter venous T_2^* at higher field strengths such as 7 Tesla (Yacoub et al., 2001) grants a lower sensitivity to vein contributions, which can introduce biases in response characterization and localization (Shmuel, Yacoub, Chaimow, Logothetis, & Ugurbil, 2007; Turner, 2002), including NBR-specific confounds (Bianciardi et al., 2011).

The aim of this work was to study the positive and negative BOLD responses elicited by visual stimulation in various regions across the brain, in humans, taking advantage of the high sensitivity of fMRI at 7T. Visual stimulation was performed with flickering checkerboards for periods of varying duration (4–40 s), while whole-brain fMRI was conducted at high spatial resolution (1.5 mm), especially relevant to study subcortical areas like the lateral geniculate nucleus (LGN), and small cortical regions such as the primary auditory cortex. Responses in visual and auditory cortex were also further investigated under visual stimulation of varying contrast (2%–80%). The study therefore extends beyond previous efforts in identification and characterization of PBRs and NBRs to visual stimulation (Laurienti et al., 2002; Shmuel et al., 2002), both in terms of spatial coverage and the range of tested stimulus durations. To further improve response estimation, a procedure for segmentation and exclusion of large draining vein contributions was also implemented in the analysis, benefitting from the high spatial

resolution and short venous T_2^* at 7T, and additional improvements were achieved via independent component analysis (ICA)-based denoising of the data.

2 | MATERIALS AND METHODS

This work was approved by the institutional review board of the local ethics committee, and involved the participation of 20 healthy volunteers (aged 23 ± 4 years old, 13 male/7 female), who provided written informed consent prior to the experiment. One half of the group participated in the main part of the work, comprising the whole-brain mapping of responses to visual stimulation, and analysis of their dependence on stimulus duration (hereafter referred to as "*Duration* study"). The second half of the group participated in an additional study focused on the responses in visual and auditory regions, analyzing their dependence on stimulus contrast (referred to as "*Contrast* study").

2.1 | Data acquisition

MRI data were acquired on a Magnetom 7T/68 cm head scanner (Siemens, Erlangen, Germany), equipped with AC84 head gradients (80 mT/m max. gradient strength, 333 T/m/s max. slew-rate) and a 32-channel receive/single-channel transmit head coil (Nova Medical, Wilmington, MA, USA). For the *Duration* study, functional data were acquired using a simultaneous multi-slice (SMS) 2D GE-EPI sequence, with TR/TE = 2000/25 ms, $\alpha = 71°$, 146 × 146 matrix size with 1.5 mm isotropic spatial resolution, 3,114 Hz/px readout bandwidth, 74 axial slices with 2× SMS acceleration and ½ field-of-view (FOV) CAIPI shift (Setsompop et al., 2012), 2× in-plane GRAPPA acceleration (anterior-posterior direction) and 7/8 partial Fourier undersampling. The resulting 11.1 cm-thick axial imaging slab allowed for whole-brain coverage excluding only part of the cerebellum. For each subject, an additional five-volume scan was performed with reversed phase encoding direction (posterior-anterior), for subsequent correction of susceptibility-induced EPI distortions. T_1-weighted anatomical data were acquired with a 3D MP2RAGE sequence (Marques et al., 2010) with TR/TI_1/TI_2/TE = 5500/750/2350/1.87 ms and 1 mm isotropic spatial resolution. For the *Contrast* study, due to unavailability of the SMS-EPI protocol, functional data were acquired using a standard 2D multi-slice GE-EPI sequence with the same volume TR, spatial resolution and in-plane acceleration, but without acceleration in the slice-encoding direction, resulting in a more restricted imaging slab (4.5 cm) with 30 slices. The slab was placed in an axial-oblique orientation to cover both the primary visual cortex and primary auditory cortex.

2.2 | Functional paradigms

All functional runs employed a series of blocks consisting of a visual stimulation period followed by a baseline period (fixation). The stimuli were delivered with an LCD projector to a screen placed at the back of the bore, and consisted of grey-scale checkerboards flickering at 8 Hz (15° FOV central-field presentation, 12 segments across the diameter), with the total luminance kept equal to baseline periods. A red cross was shown at the center of the FOV at all times, with slight changes in color occurring twice per block at random instants; subjects were instructed to focus on the cross and report color changes via a button press.

For the *Duration* study, each subject underwent two distinct paradigms: a functional localizer (*FLoc*) and a duration-varying paradigm (*FDur*). *FLoc* runs comprised 10 blocks of 10 s stimulation followed by 30 s rest; checkerboards were presented at 20% contrast. *FDur* runs comprised 30 blocks of stimulation (at 20% contrast) lasting for 4, 10, 16, 22, 30, or 40 s, followed by 30 s rest; each duration was repeated five times throughout the run, in randomized order, with the stimulus onset systematically jittered between 0 and 3.2 s, in steps of 0.8 s. For the *Contrast* study, the subjects underwent a functional localizer (*FLoc*) and a contrast-varying paradigm (*FCont*). The *FLoc* runs comprised 8 blocks of 10 s stimulation (at 20% contrast) followed by 20 s rest. *FCont* runs comprised 32 blocks of 10 s stimulation and 20 s rest, with each block of stimuli presented at one of four different contrast levels: 2%, 5%, 20%, or 80%; each level was repeated eight times throughout the run, in randomized order. These contrast levels were set based on preliminary tests, to cover a well-distributed range of (positive) response amplitudes in the visual cortex. In both studies, the *FLoc* run was used to unbiasedly identify regions of interest (ROIs) with significant responses to stimulation, which were then used for response averaging in *FDur* or *FCont* data. The protocol order was counter-balanced across subjects, and individual runs were separated by pauses of several minutes.

2.3 | Data analysis

Data analysis was mainly performed in Matlab (Mathworks, Natick MA) using routines developed in-house, combined with tools from the FMRIB Software Library (FSL v5.0, Oxford, UK) and the FreeSurfer software suite (v5.1.0, Charlestown, MA, USA).

2.3.1 | Pre-processing

Functional analysis began with motion correction (6 degrees of freedom, referenced to the middle volume of the series; Jenkinson, Bannister, Brady, & Smith, 2002), slice-timing adjustment (set to the middle of each TR, via linear interpolation), brain segmentation (Smith, 2002) and Gaussian spatial smoothing (FWHM = 2 mm). For each run, the reference volume used for motion correction was bias field-corrected with FSL-FAST (Zhang, Brady, & Smith, 2001), and used to estimate the spatial registration parameters from *FLoc* to *FDur* or to *FCont* (linear, 12 degrees of freedom [Jenkinson et al., 2002]), as well as from *FLoc* to the anatomical space (using boundary-based registration with 12 degrees of freedom [Greve & Fischl, 2009]). The anatomical image of each subject entered the standard FreeSurfer segmentation pipeline, yielding a segmentation of the cortical surfaces. No global signal subtraction or regression steps were applied at any point of the analysis.

2.3.2 | Large vein segmentation

The unsmoothed, bias field-corrected reference volume of each time-course was also used for a semi-automatic segmentation of large

draining veins. This was performed via multiscale vessel enhancement filtering (Frangi, Niessen, Vincken, & Viergever, 1998), an image-based technique that uses second-order (curvature) information to highlight vessel-like structures (Supporting Information Figure S1). Originally proposed for more dedicated angiography modalities, variants of this approach have been successfully adapted for high-spatial resolution gradient-echo fMRI data, at 3T (Koopmans, Barth, & Norris, 2010). For our 1.5 mm-resolution, 7T EPI data, the original filter (Frangi et al., 1998) was found to perform well, with empirically-determined parameters $\alpha = \beta = 0.5$, $\gamma = 0.02$, and covering spatial scales of 0.5–3.0 mm.

2.3.3 | ICA-based confound extraction

For each subject and paradigm, the pre-processed functional data were decomposed by ICA using the extended infomax algorithm (Lee, Girolami, & Sejnowski, 1999), imposing statistical independence in the spatial dimension. Data decomposition was preceded by a dimensionality reduction step using principal component analysis (PCA), where the most important components explaining 95% of total data variance were kept. Following ICA, the resulting sources were manually reviewed in search for relevant confounds, mainly related to subject motion (Kelly et al., 2010) and physiological noise (Bianciardi et al., 2009). For each dataset, the five most relevant spurious sources were selected, and their timecourses were included as confounds in subsequent regression analyses. This number of ICs was empirically found to yield a reasonably representative set of the typical artifact sources (e.g., cardiac, respiratory, residual motion, reconstruction-related), while remaining fairly conservative, which was desirable given the many features of negative BOLD responses that are still poorly understood.

2.3.4 | General linear model analysis

All pre-processed functional datasets underwent general linear model (GLM) analysis (Worsley & Friston, 1995), for the purpose of response localization (*FLoc*) and timecourse denoising (*FDur* and *FCont*). The visual paradigms were modeled as boxcar timecourses, convolved with a canonical hemodynamic response function (single-gamma function (Jezzard, Matthews, & Smith, 2001)). In *FDur* and *FCont* runs, each duration or contrast was modeled as a separate regressor. The full model comprised the visual paradigm regressors (convolved boxcars and their temporal derivatives), the button pressing task ("stick timecourse" matching the timings of button pressing, HRF-convolved), slow-drift regressors (cosine expansion covering periodicities down to 140 s), motion confounds (three translation, three rotation timecourses), and five ICA-derived confounds. For all subjects and runs, the respective models were checked for possible collinearities between the visual paradigm and confound regressors. The visual response regressors exhibited variance inflation factors below 3.6 for all models (Mumford, Poline, & Poldrack, 2015), and pairwise correlations with the confound regressors below 0.3 (one subject at 0.4). No regressor orthogonalization was applied. After GLM regression, for the *FLoc* data of each subject, a T-score map was estimated from the β map for the visual response regressor (here being the explanatory variable of interest), quantifying the significance of voxel responses to the visual paradigm.

2.3.5 | Visual response mapping

For the cortex, the mapping of responses to the *FLoc* paradigm was carried out at the subject group level, on a cortical surface space created with FreeSurfer. Only *FLoc* data from the *Duration* study were used for this purpose, due to its whole-brain coverage. First, for each subject, the *FLoc* β map for the visual response regressor was B_0-unwarped using FSL-TOPUP (Andersson, Skare, & Ashburner, 2003), and then brought to the anatomical space. The β-values were sampled by FreeSurfer throughout the cortex region, averaging across its depth, to yield a cortical surface representation of the subject's β map. The individual subject surface maps were then warped to a group average surface space, and jointly tested for statistical significance using Monte Carlo-based, cluster-wise correction for multiple comparisons, as implemented in FreeSurfer (Hagler, Saygin, & Sereno, 2006; cluster-forming threshold $|Z| > 1.6$, cluster significance $p < .01$).

2.3.6 | ROI definition and response averaging

For the cortex, a number of ROIs were defined based on the significant clusters identified by group-level analysis. At the individual subject level, the *FLoc* T-score map was also analyzed for statistical significance using topological false-discovery rate (FDR) inference (Chumbley, Worsley, Flandin, & Friston, 2010; cluster-forming threshold $|T| > 2.3$, FDR = 5%). The cluster map from group-level analysis was then brought to the subject space and compared to the FDR-thresholded T-score map, and the matching clusters were selected from the latter by visual inspection. This procedure was adopted to improve spatial specificity when localizing each cortical ROI in each subject, mitigating the impact of cross-subject misalignments and anatomical variability. A second purpose of the subject-level cluster inference was the identification of additional, sub-cortical ROIs. This was performed by visual inspection, whereby only significant clusters found consistently across subjects were selected. For the *Contrast* study, which employed a more restricted FOV, only the ROIs identified in visual and auditory cortices were considered.

Following cluster selection, each subject's ROI set was warped from *FLoc* to the *FDur* or *FCont* spaces, and any voxels belonging to segmented veins were excluded. No information from *FDur* or *FCont* was used in ROI definition, except for the vein segmentation masks. Prior to ROI response averaging, *FDur* and *FCont* data were denoised by removing drift, motion and ICA confounds, based on the corresponding GLM fits. Voxel timecourses were then baseline-corrected and normalized to a % signal change scale, and averaged across repetitions, ROIs, and subjects. For the *FDur* dataset, the jittered responses of each subject and trial were first realigned according to their relative timings, yielding an effective temporal resolution of 0.8 s, and then fit with a b-spline basis set to yield trial-average responses to each duration and subject. The order of the b-spline set was chosen so as to adequately preserve the response shapes, while excluding high-frequency noise across the aligned jittered trials.

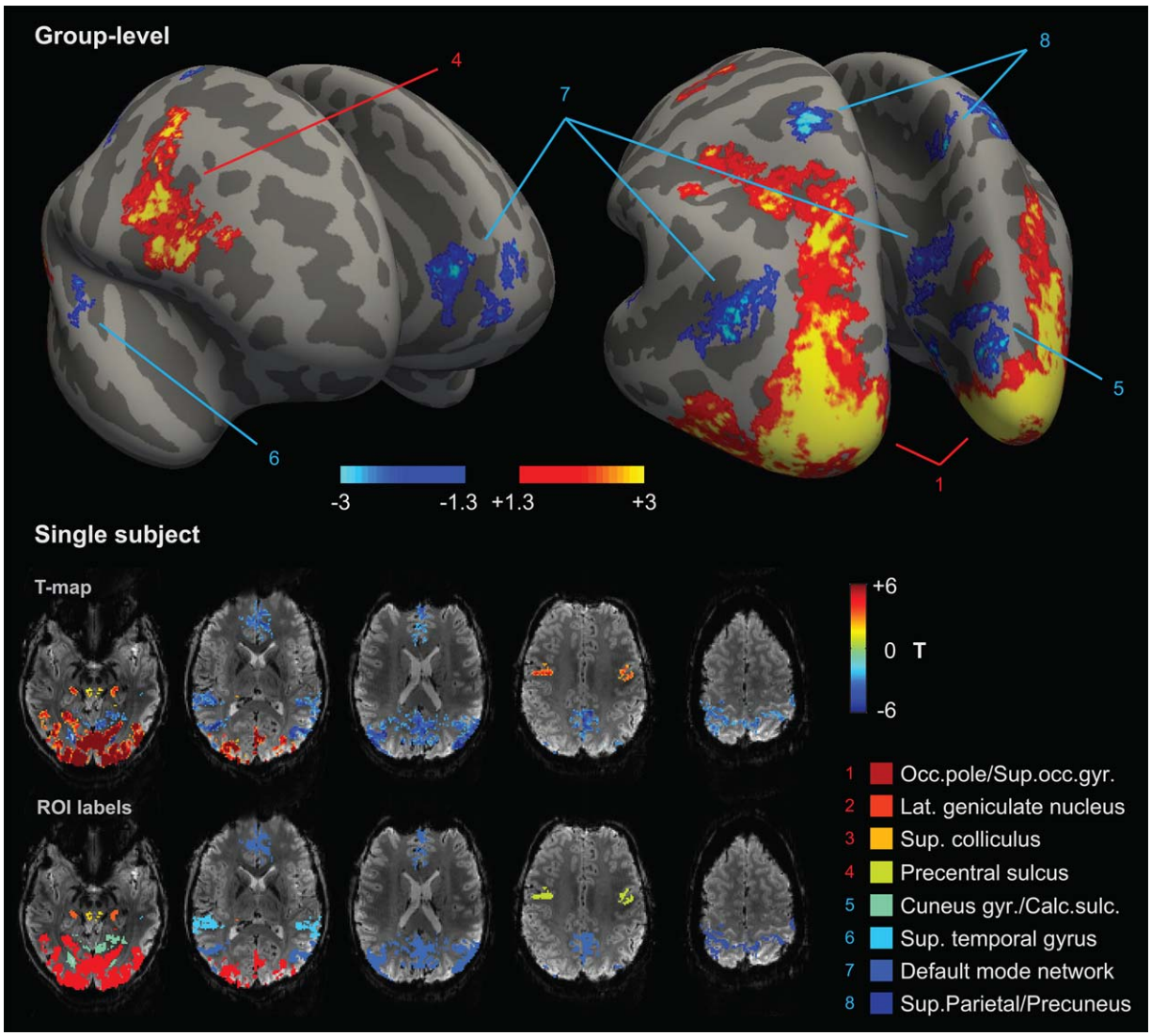

FIGURE 1 Brain-wide localization of positive and negative BOLD responses to the functional localizer paradigm (*FLoc*). Top: cortical regions identified by group-level analysis, including the occipital pole/superior occipital gyrus (1), superior/inferior pre-central sulcus (4), cuneus gyrus/calcarine sulcus (5), superior temporal gyrus (6), precuneus/posterior cingulate gyrus, angular gyrus and anterior cingulate gyrus/frontal gyrus (7), and superior parietal lobule (8); the map, rendered with FreeSurfer, is presented in $-s \log_{10}$ (p value), where s is the sign of the associated response (ex: a value of ± 1.3 corresponds to $p = .05$). Bottom: identification of the corresponding regions in an example subject, along with two sub-cortical regions: LGN (2, orange) and superior colliculus (3, yellow); each region mapped in the first row is labeled with a color index in the second row

3 | RESULTS

3.1 | Positive and negative BOLD response mapping

The *FLoc* group-level analysis revealed multiple brain regions with significant PBRs or NBRs to visual stimulation (Figure 1, Table 1). Positively-responding regions included areas V1–V4 of the visual cortex, the LGN of the thalamus, the superior colliculus, and pre-motor cortex. Negatively-responding regions included sub-parts of the primary visual cortex, primary auditory cortex, regions typically attributed to the DMN (angular gyri, precuneus and posterior cingulate gyri, medial prefrontal gyrus), and to somatosensory association cortex (superior parietal gyrus and superior precuneus gyrus, within the superior parietal lobule; Table 1). For the cortex, the identified clusters occupied 19.7% of the total cortical area—16.0% by PBRs, and 3.7% by NBRs. For some of the ROIs, not every subject exhibited a cluster on the individual T-map matching the region identified at group level; this was observed for the DMN in 2/10 subjects, the pre-motor cortex in 2/10 subjects, the superior parietal lobule in 2/10 subjects, and the superior colliculus in 3/10 subjects. For these cases, the subjects were excluded from the averaging for the respective ROI.

3.2 | Positive and negative BOLD stimulus dependence

Under varying stimulus duration (*FDur* paradigm), the group-average BOLD responses exhibited clear stimulus dependence, with response duration tending to increase with stimulus duration in all ROIs (Figure

TABLE 1 Brain regions with significant positive or negative BOLD responses to visual stimulation

Sign	Anatomical region	Brodmann area	Putative function	Peak Z (group level)
+	Occipital pole Sup. occipital sulcus	17,18,19	Visual	+5.7
+	Precentral sulcus	6	Pre-motor (behavior control, movement planning)	+4.9
+	Lat. geniculate nucleus	–	Visual	–
+	Sup. colliculus	–	Oculomotor control	–
−	Cuneus gyrus Calcarine sulcus	17,18,19	Visual	−4.0
−	Sup. temporal gyrus	41,42	Auditory	−3.1
−	Angular gyrus	39	Default mode network	−4.4
−	Precuneus gyrus Post. cingulate gyrus	23	Default mode network	−3.7
−	Medial prefrontal gyrus	10	Default mode network	−4.0
−	Sup. parietal lobule	5,7	Somatosensory association	−4.6

Note: Cortical regions were identified at the group level by cluster-wise inference (cluster-forming threshold $|Z| > 1.6$, cluster $p < .01$, FWE-corrected); anatomical labeling was based on the FreeSurfer atlas. Subcortical regions were identified by visual inspection of cluster-thresholded, FWE-corrected T-score maps at the individual subject level.

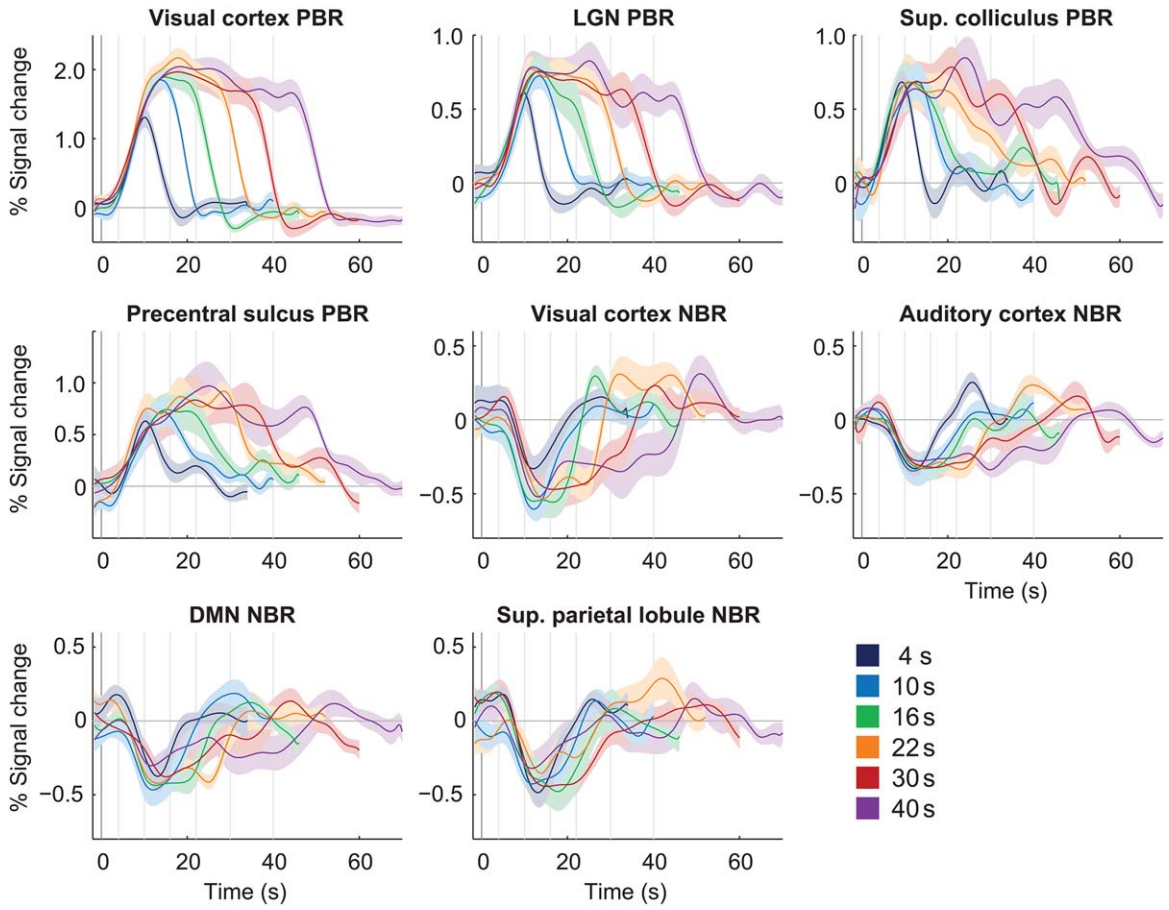

FIGURE 2 Group average BOLD responses to 20%-contrast checkerboard stimulation with varying duration (*FDur*), in multiple brain regions. The response curves represent average responses across subjects, with error margins representing the respective standard error; vertical lines mark the instant of stimulus cessation for each duration [Color figure can be viewed at wileyonlinelibrary.com]

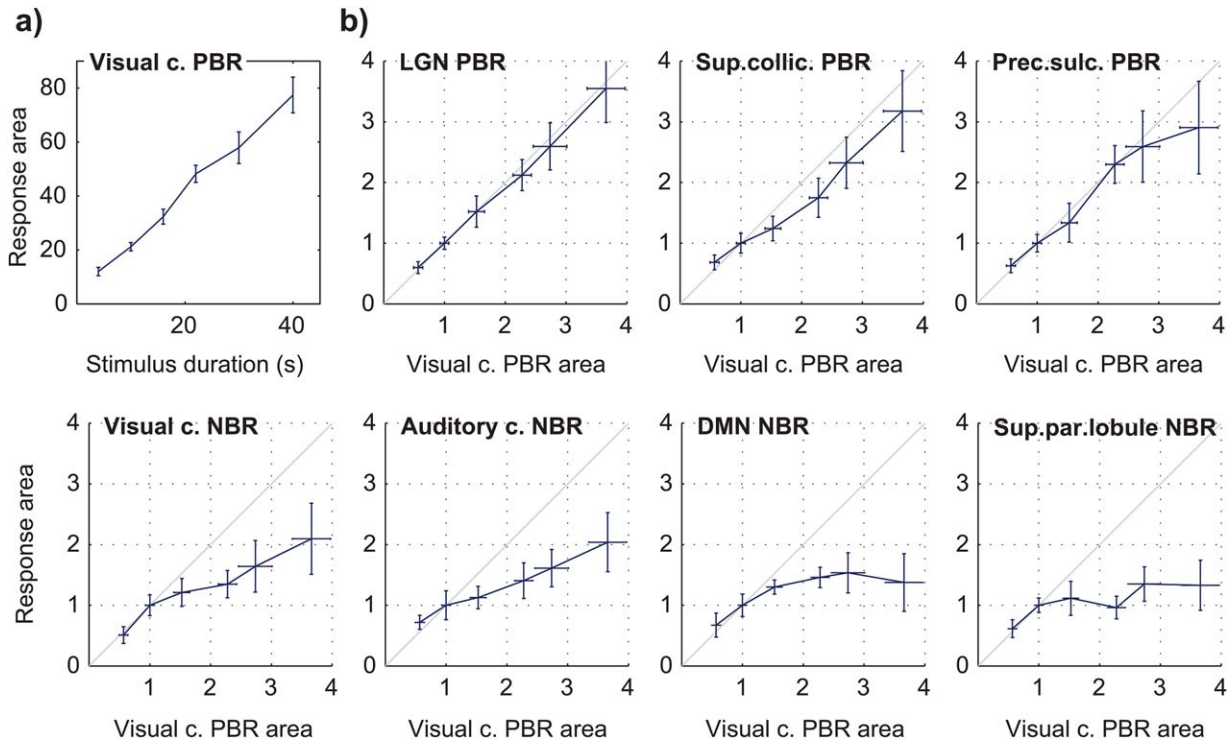

FIGURE 3 Group average BOLD response durations to 20%-contrast checkerboard stimulation with varying duration (*FDur*), in multiple brain regions. Each response duration was estimated as the area under the response curve. (a) Duration of the visual cortex PBR as a function of stimulus duration. (b) Response durations in the other identified regions of interest, plotted as a function of the visual cortex PBR duration, after normalization to the response area at 10 s stimulation; the diagonal grey line marks the identity function. All response durations represent averages across subjects, with error bars representing the standard error [Color figure can be viewed at wileyonlinelibrary.com]

2). Overall, no differences in response properties were found between hemispheres, and as such the two hemispheres were analyzed together for each ROI; the same was observed for the various regions of the DMN, which were thereby also merged.

Certain ROIs were visibly less affected by stimulus duration than others. In particular, the NBR regions tended to exhibit less sustained responses than the visual cortex PBR, especially evident for the longer stimulation conditions (Figure 2). Response duration was quantified by normalizing the response amplitude and estimating the area under the response curve for each stimulus duration, excluding the under/overshoot and subsequent periods. Based on this measure, the visual cortex PBR duration was found to increase close to linearly with stimulus duration (offset = 4.2, slope = 1.8 s^{-1}; Pearson coefficient $r = .90$ with $p < .01$, Figure 3a). In general, duration dependence was found statistically significant for all PBR regions, as well as the visual and auditory cortex NBRs ($p < .05$ for the effect of stimulus duration, balanced one-way ANOVA), but not for the DMN and superior parietal lobule. The response areas for each ROI were further compared to the visual cortex PBR across stimulus durations, after being normalized to the respective values for 10 s stimulation (Figure 3b). No significant deviations between any ROI response areas and the visual cortex PBR were found for stimuli up to 16 s; however, for longer stimulus durations, the response areas from all NBR regions were found significantly smaller than that of the visual cortex PBR ($p < .01$, balanced one-way ANOVA).

The BOLD response time of return to baseline and time to peak were also estimated for each subject, duration and ROI. These timings were obtained by modeling the individual responses with a combination of inverse logit functions (Lindquist & Wager, 2007), to capture the general response shapes while excluding smaller artifactual fluctuations, for a more robust estimation. As observed for the response areas, the time of return to baseline increased with stimulus duration in all regions (Figure 4a). A linear increase with stimulus duration was again found for the visual cortex PBR (offset = 12.9, slope = 0.9 s^{-1}; $r = .95$ with $p < .01$). In NBR regions, the return to baseline tended to occur earlier compared to the visual cortex PBR, especially for stimuli above 16 s ($p < .01$ for the visual cortex NBR and superior parietal lobule NBR, balanced one-way ANOVA). The time to peak was, in general, found to increase moderately with stimulus duration, up to around 30 s durations (Figure 4b). Most regions peaked at approximately the same time as the visual cortex PBR, with three exceptions: the auditory cortex NBR tended to peak approximately 4.3 s later, consistently across stimulus durations ($p < .01$, balanced one-way ANOVA); the pre-central sulcus PBR and DMN NBR both tended to peak increasingly later than the visual cortex PBR for increasing stimulus duration ($p < .05$, balanced one-way ANOVA).

Under contrast-varying stimulation (*FCont* paradigm), group-average BOLD responses exhibited clear stimulus dependence in all three targeted ROIs (visual cortex PBR, visual cortex NBR and auditory cortex NBR), with response peak amplitudes increasing monotonically

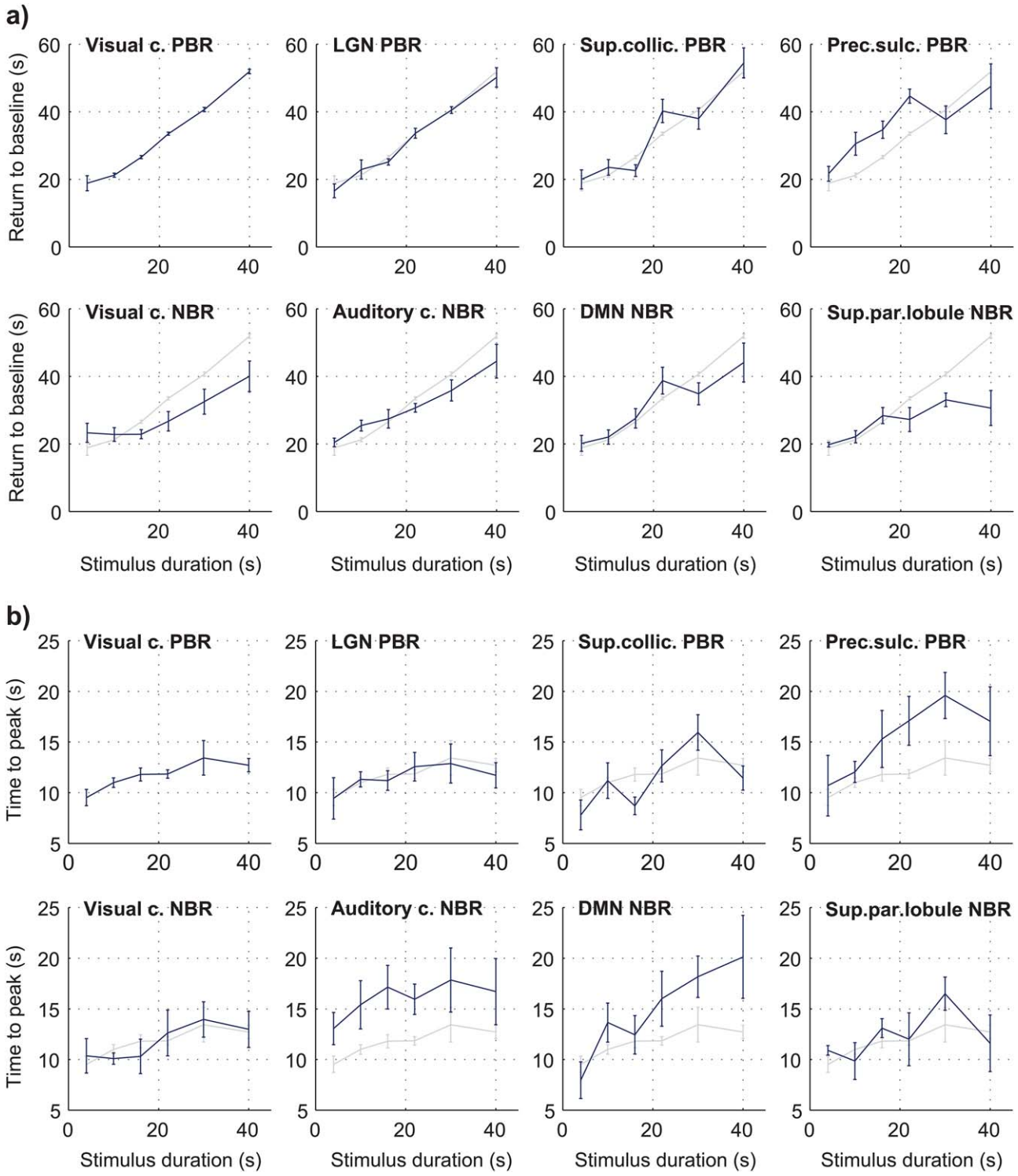

FIGURE 4 Group average BOLD response properties as a function of stimulus duration (*FDur*), in multiple brain regions. Individual subject responses were modeled as a combination of inverse logit functions (Lindquist & Wager, 2007) for a more robust estimation of (a) the time of return to baseline, and (b) the time to peak, both measured relative to the onset of stimulation. All estimates represent averages across subjects, with error bars representing the standard error. Because they do not depend on the response amplitudes, the response timings did not need to be normalized (as performed for response areas). Instead, the visual cortex PBR curve is also shown in light grey in every panel, for direct comparison with each region [Color figure can be viewed at wileyonlinelibrary.com]

with checkerboard contrast (Figure 5a). The contrast dependence of response amplitudes was statistically significant for all ROIs ($p < .05$ for the effect of stimulus contrast, balanced one-way ANOVA). NBRs were then compared to the visual cortex PBR by normalizing each set relative to its 20% contrast response amplitude. This procedure revealed a linear correlation between both visual and auditory NBR amplitudes

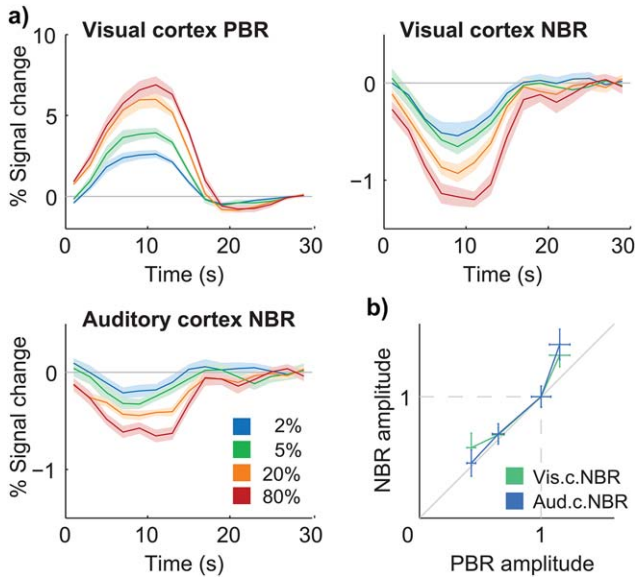

FIGURE 5 Group average BOLD responses to 10 s-checkerboard stimulation with varying contrast (*FCont*). (a) Visual cortex PBRs (top–left), visual cortex NBRs (top–right) and auditory cortex NBRs (bottom–right) to four increasing contrast levels. (c) Visual and auditory cortex NBR amplitude as a function of visual cortex PBR amplitude, after normalization of each response to the amplitude at 20% contrast; the diagonal grey line marks the identity function. All response curves and amplitudes represent averages across stimulation blocks and subjects, with error margins and bars representing the standard error across subjects [Color figure can be viewed at wileyonlinelibrary.com]

and the visual PBR amplitude, at least for contrast levels up to 20% (Figure 5b). Within this range, pooling together the response amplitudes from all subjects and the three lowest contrast levels, without normalization, a linear relationship was observed between the visual cortex PBR amplitude and both visual cortex NBR ($r = -0.50$, with $p < .05$) and auditory cortex NBR amplitudes ($r = -0.55$, with $p < .05$). At 80% contrast, both normalized NBRs displayed a comparable deviation from the PBR, with stronger relative increases in amplitude (Figure 5b). Overall, the two NBR types exhibited a similar dependence on stimulus contrast, although with the visual NBR achieving larger amplitudes in general.

Overall, for both varying stimulus duration and contrast, the observed responses exhibited appreciable differences across regions and stimuli, not only in amplitude and duration, but also in shape. Notably, response under/overshoots could be observed in most regions (Figure 2), but not all (superior colliculus and pre-central sulcus PBRs). Where present, the average response under/overshoots tended to occur later for longer stimulus durations. Although no clear differences in under/overshoot peak timing could be found across regions, the peak amplitude was notably stronger in both visual cortex responses than elsewhere (Supporting Information Figure S2). Interestingly, the under/overshoot peak amplitude varied considerably across stimulus durations, and was particularly weak in visual and auditory regions for the 10 s-stimuli; consistently, in the contrast-varying data, which employed the same duration, the observed under/overshoots were likewise relatively weak (Figure 5). The trends observed for the main response amplitudes in *FCont* were, nevertheless, fairly robust to minor shape variations; in particular, an alternative quantification of these trends based on the response areas, instead of peak amplitude, yielded the same relationship between PBRs and NBRs (results not shown).

3.3 | Grey matter—vein separation

To assess the impact of vein contributions to BOLD response characterization, the voxels identified as large draining veins were analyzed separately and compared to those attributed to grey matter, in the *Contrast* study. Visual inspection of *FLoc* Z-score maps across subjects identified several small clusters (1.5–4.5 mm diameter) dominated by a central Z-score peak, spatially coincident with a large draining vein (Figure 6a). Consistent with previous reports at 7T (Yacoub et al., 2001), responses to visual stimulation from vein-identified regions were considerably stronger than in grey matter — in visual cortex, for instance, the average venous baseline signals were approximately 0.6× those of grey matter, yet their PBRs displayed absolute signal changes that were 1.5× stronger, resulting in even stronger % signal changes (approximately 2.6× higher than in grey matter). Furthermore, visual cortex PBRs were visibly delayed in veins relative to grey matter (Figure 6b). While the available temporal resolution did not allow for proper quantification of the temporal delay, this effect was robustly observed in visual cortex PBRs for all contrast levels, as well as in NBRs to higher contrasts. Finally, although roughly expressing similar trends, the stimulus dependence of venous responses was considerably more irregular than in grey matter, especially for NBRs (Figure 6c). Upon merging vein and grey matter ROIs for each response type (as would happen if no vein separation had been applied), response amplitudes remained roughly similar to those of "pure" grey matter for visual PBRs and NBRs, but showed relevant perturbations for auditory cortex NBRs (results not shown). Concordantly, in the merged ROIs, the effect of stimulus contrast became less statistically significant in general (larger *p* values).

3.4 | ICA-assisted denoising

The impact of ICA-assisted denoising on data quality was assessed based on both the variance explained by ICA confounds and their effect on block-by-block response variability, for *FLoc* data. Systematically across subjects, the ICA decomposition produced components that could be clearly identified based on their spatial distribution and/or temporal properties, such as paradigm-related sources, resting-state networks, and physiological noise sources related to cardiac or respiratory processes (Supporting Information Figure S3).

The proportions of data variance explained by the paradigm, head motion and ICA confounds were estimated based on the adjusted coefficient of determination (R^2_{adj}) obtained from the residuals of GLM analysis (Jorge, Figueiredo, van der Zwaag, & Marques, 2013). Across subjects and brain regions, the ICA confounds proved to explain significant amounts of data variance ($p < .01$, one-sample *t* tests), averaging approximately 17% in visual cortex PBR ROIs, 16% in visual cortex

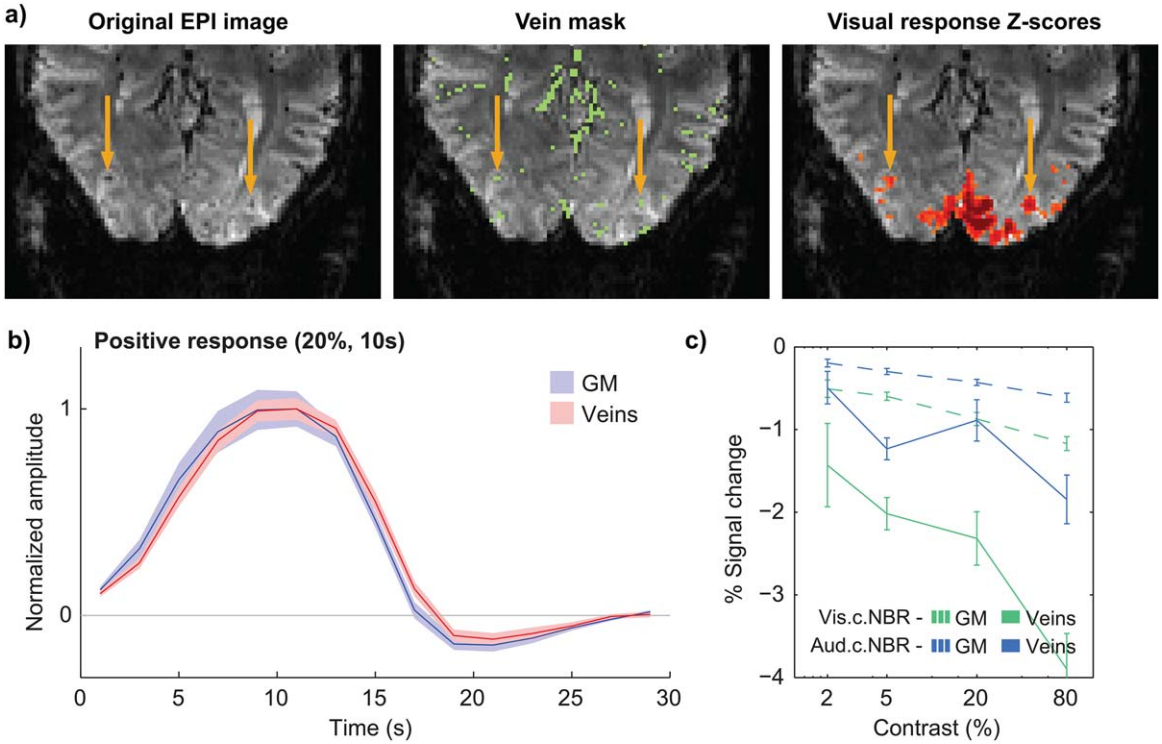

FIGURE 6 The influence of large draining veins on response localization and temporal characterization. (a) GE-EPI data from a single subject (left), the respective vein mask obtained with multiscale vessel enhancement filtering (center), and a thresholded T-score map for the visual cortex response to the functional localizer; yellow arrows indicate two veins which are positioned in the center of activation clusters, exhibiting large Z-scores. (b) Group average visual cortex PBRs to checkerboard stimuli of 20% contrast and 10 s duration, in grey matter (blue) and segmented vein voxels (red). (c) Group average peak amplitude of visual and auditory cortex NBRs to varying contrast level, in grey matter and in segmented veins; the horizontal axis (stimulus contrast) is presented in logarithmic scale for easier visualization. All response curves and amplitudes represent averages across stimulation blocks and subjects, with error margins and bars representing the standard error across subjects [Color figure can be viewed at wileyonlinelibrary.com]

NBR ROIs, and 15% in auditory cortex NBR ROIs, for example (Figure 7a). These proportions of explained variance were generally larger than those achieved by the head motion confounds, and even larger than those of the paradigm responses for the weaker NBRs, such as the auditory cortex case. To assess block-by-block response variability, for each subject, considering ROI-averaged BOLD timecourses, the standard deviation across blocks was computed for each timepoint of the response window, and then averaged across timepoints. On average, the inclusion of ICA confounds in the regression models led to further reductions in block-by-block response variability compared to the use of motion regressors alone. Together, these confounds significantly reduced variability by approximately 19% in visual cortex PBR ROIs, 17% in visual cortex NBR ROIs, and 19% in auditory cortex NBR ROIs, for example ($p < .01$, one-sample t tests; Figure 7b).

4 | DISCUSSION

The present study explored the high functional sensitivity available at 7T, combined with accelerated fMRI acquisition, vein segmentation and ICA denoising techniques, to map and characterize both positive and negative BOLD responses to visual stimulation throughout the brain. Multiple areas exhibiting significant responses to visual stimulation were found, and their dependence on stimulus duration was observed to differ significantly across regions. The exclusion of large-vein contributions and ICA-derived confounds was shown to significantly improve response estimation.

4.1 | Positive and negative BOLD response mapping

Recent fMRI studies based on large single-subject datasets have revealed that even passive checkerboard stimuli can elicit sustained BOLD responses in more than 50% of all grey matter—with roughly 41% positive, and 13% negative responses (Gonzalez-Castillo et al., 2015). This compelling observation suggests that valuable new insights may be achieved through the mapping of both PBRs and NBRs on a whole-brain scale, even for fairly basic stimuli, opening new perspectives for the study of brain function. However, such descriptions required long acquisitions with hundreds of block repetitions per subject, limiting a more widespread applicability. The large gains in functional sensitivity achieved at higher field strengths can help to mitigate this obstacle, which is particularly decisive for NBR detection. A trade of sensitivity for spatial resolution can also help studying small structures such as the LGN, and negative responses in small cortical regions, such as the auditory cortex NBR, will crucially benefit from both sensitivity and spatial specificity. Recent developments in slice-accelerated 2D-EPI have brought excellent trade-offs between sensitivity, spatial

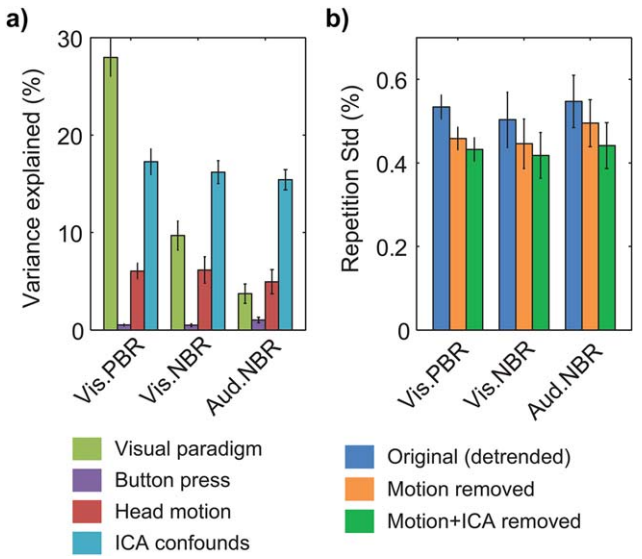

FIGURE 7 The impact of the different subsets of regressors included in GLM analysis, exemplified for the functional localizer data (*FLoc*) in visual cortex PBR, visual cortex NBR and auditory cortex NBR regions. (a) Average percentages of data variance explained by the visual paradigm (green), button pressing to track changes in the central cross (purple), head motion (red) and ICA-based confounds (blue). (b) Block-by-block response variability, expressed in % signal change, before (blue) and after removal of head motion regressors (orange) and head motion + ICA-based confounds (green). The bars indicate averages across subjects, with error margins representing the respective standard error. The variance that remains unaccounted for is putatively attributed to residual artifact contributions, spontaneous activity and trial-by-trial fluctuations (Mayhew et al., 2016), and thermal noise. Low frequency (drift) contributions, as modeled within the GLM, were excluded prior to these estimations, and therefore do not contribute to the total variance or variability here presented [Color figure can be viewed at wileyonlinelibrary.com]

and temporal resolution (Setsompop et al., 2012), and were exploited in this work to achieve whole-brain coverage at a reasonable volume TR of 2 s, with a spatial resolution of 1.5 mm—which matches the specificity limits estimated for single-condition BOLD response mapping at 7T (Shmuel et al., 2007). In this regime, our checkerboard paradigm comprising only 10 stimulus repetitions, lasting less than 7 min in total, revealed significant BOLD responses in almost 20% of grey matter, with PBRs and NBRs appearing in similar relative proportions to those found by Gonzalez-Castillo et al. (2015).

The detection of PBRs to visual stimulation in the primary visual cortex, LGN and superior colliculus is expected, as the first two are well-known components of the visual pathways, and the latter is involved in oculomotor control (Guyton & Hall, 2006). NBRs to visual stimuli have also been reported for regions of the visual cortex (Shmuel et al., 2002) and auditory cortex (Laurienti et al., 2002). In the DMN, NBRs are often observed in more demanding cognitive tasks, such as involving arithmetic operations (Lin et al., 2011) or working memory (Mayer et al., 2010), but this is, to our knowledge, the first report of their robust detection in a passive flickering checkerboard paradigm. Previous studies employing analogous passive stimuli at 3T have reported NBRs in posterior cingulate and medial prefrontal cortex (Mayhew et al., 2013), though not unanimously (Greicius, Krasnow, Reiss, & Menon, 2003), possibly due to the lower functional sensitivity at this field strength. Other differences relative to previous reports suggest that the observed responses may also be considerably specific to the properties of the visual stimuli; for example, while our basic checkerboard stimuli yielded NBRs in the auditory cortex (similar to the findings of Laurienti et al. (2002)), Kayser, Petkov, Augath, and Logothetis, (2007) found auditory PBRs in monkeys when watching natural scenes of animal wildlife. This interesting example suggests that visual stimuli with contextual significance, and associated representations in other sensory areas, may trigger different cognitive mechanisms and multisensory interactions, with noticeable effects on the observed BOLD responses.

The PBR observed in the pre-central sulcus suggests an involvement of pre-motor cortex in the response to the visual stimuli. While this region's functions remain poorly understood, neurons in its ventral portion are known to respond to visual stimuli appearing in positions close to the body, possibly related to hand-reaching functions (Graziano, Yap, & Gross, 1994). Certain parts of pre-motor cortex are also involved in the association between arbitrary visual stimuli and motor responses (Brasted & Wise, 2004) and in movement-related decisions (Deiber et al., 1991). Considering that the subjects were tasked with focusing on a central cross and pressing a button whenever its color changed, throughout the paradigm, one could speculate that the presentation of checkerboards could trigger responses in this region as an interfering "distracter", arising as the participant was alert for cross changes. The occurrence of NBRs in the superior parietal lobule is also, to our knowledge, a novel finding, although the somatosensory association cortex (located in these regions) has previously been found to respond to changes in ongoing visual stimulation (Downar, Crawley, Mikulis, & Davis, 2000). On the other hand, this area can also be involved in visuomotor coordination processes (Deiber et al., 1991). Thus, these questions could potentially be clarified in future studies by employing a similar checkerboard paradigm with a different visuomotor attention task, or none, for example.

Overall, the detection of NBRs in various regions distributed throughout the brain suggests a functionally-relevant meaning for these responses. For example, the auditory cortex and DMN are spatially well separated from the visual cortex, and thus their NBRs are unlikely to be caused by passive "vascular steal" effects—an observation analogous to those of previous works reporting ipsilateral NBRs to tactile stimulation (Hlushchuk & Hari, 2006; Kastrup et al., 2008; Klingner et al., 2010) and to motor tasks (Hamzei et al., 2002; Stefanovic et al., 2004). This strengthens the hypothesis of a local neuronal origin for negative BOLD, or alternatively the existence of long-range vascular control mechanisms that could modulate CBF across cortical regions (Smith et al., 2004; Vafaee & Gjedde, 2004).

4.2 | Positive and negative BOLD stimulus dependence

The stimulus dependence of visual cortex NBRs to visual stimuli has been previously shown for stimulus duration (up to 16 s) and intensity

(Shmuel et al., 2002). As for NBRs to visual stimulation in other brain regions (cross-modal responses), their dependence on stimulus properties remains largely unexplored, and was here studied for the first time for stimulus duration, and in the case of the auditory cortex, for stimulus contrast as well. Visual and auditory cortex NBR amplitudes were found to increase with stimulus contrast, and NBR durations were also generally found to increase with stimulus durations up to 16 s, in all studied regions. Under the hypothesis of local neuronal deactivation, these findings would imply that deactivation increases with stimulus intensity and is more prolonged with longer stimuli. Alternatively, the long-range CBF control hypothesis could either imply a stimulus-dependent CBF reduction, without changes in neuronal activity, or an unvarying suppression of CBF changes with stimulus-dependent increases in neuronal activity.

For stimulus durations of 16 s and above, all NBRs tended to be less sustained than the visual cortex PBR (Figure 2), leading to growing deviations from linear covariation (Figure 3). The return to baseline of NBRs also tended to occur earlier than that of the visual cortex PBR, and various regions exhibited significantly different behaviors in response peak timing, both stimulus-dependent and independent. These phenomena have not been reported in previous work studying the visual cortex NBR, which explored stimulus durations only up to 16 s (Shmuel et al., 2002). On the other hand, in tactile stimulation studies using longer stimuli (20 s), ipsilateral somatosensory cortex NBRs have likewise been found to decay faster than contralateral PBRs (Hlushchuk & Hari, 2006). The mechanisms underlying the observed effects cannot be fully understood based on these data alone; nevertheless, they suggest either the existence of differences between the hemodynamic coupling mechanisms of PBRs and NBRs, which become more evident for sufficiently long stimuli, or the possibility that neuronal deactivation does not closely follow the same temporal dynamics of neuronal activation. The possibility of hemodynamic coupling differences between PBRs and NBRs has been previously suggested by work in both visual (Shmuel et al., 2002) and median nerve stimulation (Mullinger et al., 2014), arising as differences in the ratio of $\Delta CMRO_2$ to ΔCBF, but has not been found in the motor cortex (Stefanovic et al., 2004) or DMN (Lin et al., 2011). This latter reference, focused on the DMN, also employed fairly long task durations, albeit with a more cognitively-demanding task than that used in this work. It is important to note that, because the observed responses were located in different regions across the brain, the deviations found in their temporal dynamics could, at least partially, be due to regional differences in hemodynamic coupling, namely regarding BOLD response habituation, and not necessarily specific to the type of response (positive or negative). While one could attempt to use different stimuli to elicit and study PBRs in the same regions where NBRs were identified for this work, this would still not fully disentangle this uncertainty, because habituation mechanisms can also be stimulus specific. Nevertheless, for the range of stimuli explored in this work, all PBR regions exhibited response durations that closely followed the stimulus duration, showing no discernible signs of habituation (Figure 3a,b and 4a). In contrast, all NBR regions tended to deviate from this behavior, suggesting that the observed effects are more likely to be response-related, rather than purely region-specific.

Following the hypothesis of differences at the level of neuronal activity, an attenuation of the neuronal deactivation response for longer stimuli could suggest the existence of mechanisms which downplay the importance of visual stimuli when these are presented for sufficiently long periods of time. Neuronal responses can suffer from habituation effects for sufficiently long stimuli (Janz, Heinrich, Kornmayer, Bach, & Hennig, 2001). Here, however, the visual cortex PBR did not evince signs of habituation (Figure 3a), and the NBRs were found to be less sustained relative to the PBR itself, implying differences in the hypothetical adaptation mechanisms attenuating the neuronal deactivation in NBR regions, compared to those attenuating neuronal excitation in PBR regions. Also importantly, for most NBR regions under study, except possibly the superior parietal lobule, the observed response curves did not appear to reach a plateau in terms of response duration, suggesting that, at least for stimulus durations up to 40 s, such attenuation mechanisms, if present, do not effectively reach a full suppression of the deactivation response.

Besides region-specific differences in response habituation, another potential source of variability may have had a relevant impact on the observed response properties: as shown by Mayhew et al. (2016), and contrasting with their trial-average relationship (Figure 5), PBRs and NBRs from different brain regions can exhibit fluctuations in amplitude across trials that are positively-correlated (i.e., when the PBR becomes more positive, the NBR also becomes more positive, and vice-versa). These positively-correlated trial-varying contributions introduce variability on the observed BOLD responses across trials, and more importantly, they could have a relatively larger impact on the weaker responses than on the visual cortex PBR, possibly influencing the observed PBR and NBR relationships. We sought to assess the potential impact of this confound through numerical simulations, focusing on response area estimation for the weakest response regions (superior colliculus PBR and auditory cortex NBR), in the presence of positively-correlated random spurious fluctuations. The BOLD responses were simulated based on the paradigm regressors, i.e., as if having the same stimulus dependence in all regions (Supporting Information Figure S4a), and the response amplitudes and spurious variability were scaled according to the observed data (Figure 2 and Figure 7b). The presence of spurious contributions was indeed found to exert an observable effect on the response relationships (Supporting Information Figure S4b), and could explain the small deviation observed for the superior colliculus PBR (Figure 3), which however was not statistically significant. In contrast, the stronger deviations observed for the NBRs were well beyond the range of simulated outcomes, and therefore could not be explained by positively-correlated fluctuations. Nevertheless, these results show that such contributions can be an important source of variability, and could potentially affect PBR-NBR comparisons in a systematic manner for certain analyses; they should therefore not be disregarded in this type of studies.

Under contrast-varying stimulation, response amplitudes showed a tight correlation between the visual cortex NBR and PBR, for contrast levels up to 20% (Figure 5b). This is consistent with previous

observations at similar contrast ranges, up to 40% (Shmuel et al., 2002). Notably, the auditory cortex NBR was also strongly correlated to the visual cortex PBR, suggesting similar underlying neuronal interactions for both NBR types, and analogous hemodynamic coupling. At 80% contrast, the visual cortex PBR did show a lower relative increase than either the visual or auditory cortex NBRs (Figure 5). This interesting behavior could potentially be due to differences in the limits for response saturation, and could be tested in future work by exploring even stronger stimulus intensities, which may push both positive and negative responses to clear saturation plateaus.

Given the steadily-growing body of evidence associating negative BOLD with true local neuronal deactivation (Boorman et al., 2010; Mullinger et al., 2014; Pasley et al., 2007; Shmuel et al., 2006), this hypothesis is a strong candidate under which to interpret the observed NBRs and their dependence on basic stimulus properties. Under that assumption, these results point to the existence of highly dynamic cross-modal neuronal interactions that depend on stimulus intensity and duration, occurring in various regions of the brain, even under passive viewing of basic visual stimuli. Future studies monitoring both BOLD and electrophysiological activity, in both PBR and NBR regions, may bring valuable additional insights to clarify this idea, and to further our current understanding of the neurovascular coupling mechanisms underlying the BOLD signal in general.

The results obtained in this work also suggest that manipulating stimulus duration could be an effective, and fairly straightforward way to create situations of decoupling between positive and negative responses, and this effect could be explored to study particular aspects of their relationship. From a more practical standpoint, these results also point to the need of careful response modeling when studying PBRs and NBRs, which may be particularly critical for longer stimulus durations (in this case, checkerboard stimuli longer than 16 s). Parameters such as the response area, peak timing, return to baseline and under/overshoot showed clear deviations between PBRs and NBRs, as well as across different stimuli in the same region. The inclusion of temporal and dispersion derivatives to the canonical HRF models can offer some flexibility regarding the delay and width of the main response peaks, but more flexible approaches such as finite impulse response or Fourier basis set modeling may be necessary to account for more particular response features, as long as the concomitant losses in detection power and interpretability remain acceptable. In this work, we used a canonical HRF model for response mapping, relying on the high detection power of block designs to ensure robustness against modeling errors. Response characterization was performed either directly on the observed average responses, or aided by modeling with inverse logit functions (Lindquist & Wager, 2007), which also showed a favorable tradeoff between flexibility and robustness, and could be a pertinent option for future studies as well.

4.3 | Grey matter—vein separation

Draining veins are known to influence response localization (Barth & Norris, 2007) and can propagate activity-related changes in blood oxygenation for several mm downstream from activation sites (Turner, 2002). Furthermore, as vein-propagated responses are delayed in time relative to the original activation site, their contributions to response averaging can affect the temporal properties of the responses of interest (Shmuel et al., 2007). Thus, although less influent at 7T than at lower field strengths (Yacoub et al., 2001), venous contributions are undesirable, especially for the characterization of lower-contrast responses such as NBRs.

Various approaches for vein identification in fMRI have been proposed (Barth & Norris, 2007; Koopmans et al., 2010; Menon, 2002). Given the high spatial resolution available at 7T, and decreased venous T_2^*, large veins are clearly discernible as dark, focal susceptibility artifacts in the functional data, motivating the use of image-based segmentation approaches. To our knowledge, this is the first study applying multiscale vessel-enhancement directly on GE-EPI data, an approach which presents several advantages: (i) it avoids the acquisition of separate "vein-sensitized" images, and the necessary co-registration steps to fMRI data, which need to be highly accurate for correct vessel localization; (ii) being an image-based method, it can be easily optimized through visual inspection; and (iii) the method is applied retrospectively, with no specific requirements imposed on the acquisition (apart from sufficient spatial resolution). It should be noted that this segmentation approach does not yield actual venograms, as the susceptibility artifacts created by veins expand beyond the vessels into adjacent tissues. While lowering the specificity of segmentation, this effect is actually advantageous as it allows the detection of vessels thinner than the available spatial resolution, and can lead to more conservative response estimations in grey matter, as tissues with T_2^* perturbations due to the proximity of veins are likewise excluded.

In this work, the influence of veins in both response localization and characterization could be clearly observed (Figure 6a,b). Moreover, the stimulus dependence of venous ROIs, segmented as described above, was considerably less regular than that of grey matter ROIs (Figure 5c), potentially due to their inherently poorer response specificity and/or to a higher sensitivity to subject motion and physiological noise. Moreover, when combining venous and grey matter responses together as if no vein separation had been performed, the stimulus dependence of merged responses also became less regular than in grey matter alone. These effects support that vein separation is indeed highly desirable when studying BOLD responses of low amplitude and/or occurring in small brain regions.

4.4 | ICA-assisted denoising

ICA has been extensively explored for fMRI data analysis and denoising (Smith et al., 2013), and can be combined with methods for automatic source classification (Griffanti et al., 2014; Salimi-Khorshidi et al., 2014). In this work, we opted for manual source selection performed under fixed criteria (Kelly et al., 2010; van der Zwaag et al., 2009b), to ensure that no paradigm-related sources were taken. The timecourses of the selected ICs were then included as confounds in GLM regression, as often done for motion and physiological noise (Bianciardi et al., 2009), thus unifying response detection and noise modeling in the GLM analysis stage. The performance of ICA-assisted denoising was

assessed based on the data variance explained by ICA regressors, and their impact on response variability. The first measure relied on estimating R^2_{adj}, which allows for unbiased comparisons between models with different numbers of regressors. The second measure is not independent of the number of degrees of freedom, but provides a more direct indication of improvements in response denoising. As exemplified for visual and auditory cortex responses, the ICA-based confounds were found to explain significant proportions of data variance, superior to those of head motion confounds, and were especially important for the NBR ROIs, where the paradigm contributions were smaller than those of the confounds. Concordantly, reductions in block-by-block variability were significant for all responses, and are particularly relevant for NBR estimation, given their smaller amplitude. Overall, the use of ICA-derived confounds proved to be a valuable approach, which can complement or even replace other techniques targeting correlated noise sources, such as physiological noise modeling based on external monitoring.

5 | CONCLUSION

Ultra-high field fMRI, explored using accelerated EPI acquisition, combined with vein segmentation and ICA denoising, allows the robust detection of positive and negative BOLD responses to visual stimulation in various brain regions within and beyond the visual cortex, even with a paradigm lasting only a few minutes per subject. Under stimuli of varying duration and intensity, both positive and negative responses can exhibit important region-specific differences in stimulus dependence. In the light of growing evidence associating negative BOLD with local neuronal deactivation, these findings suggest the existence of dynamic cross-modal neuronal interactions that depend on stimulus intensity and duration, involving various regions of the brain, even under passive viewing of basic visual stimuli. In data analysis, the exclusion of large-vein contributions and correlated noise confounds can significantly improve BOLD response estimation, boosting sensitivity and specificity.

ACKNOWLEDGMENTS

This work was supported by Centre d'Imagerie BioMédicale (CIBM) of the UNIL, UNIGE, HUG, CHUV, EPFL and the Leenaards and Jeantet Foundations, the Swiss National Science Foundation through grant #31003A-153070, and by the Portuguese Science Foundation (FCT) through grants SFRH/BD/51449/2011, PTDC/EEI-ELC/3246/2012 and PEst-OE/EEI/LA0009/2013.

DISCLOSURE/CONFLICT OF INTEREST

The authors declare no conflict of interest.

ORCID

João Jorge http://orcid.org/0000-0001-6667-1868

REFERENCES

Andersson, J. L., Skare, S., & Ashburner, J. (2003). How to correct susceptibility distortions in spin-echo echo-planar images: Application to diffusion tensor imaging. *Neuroimage*, *20*(2), 870–888.

Barth, M., & Norris, D. G. (2007). Very high-resolution three-dimensional functional MRI of the human visual cortex with elimination of large venous vessels. *NMRi N Biomedicine*, *20*(5), 477–484.

Bianciardi, M., Fukunaga, M., van Gelderen, P., de Zwart, J. A., & Duyn, J. H. (2011). Negative BOLD-fMRI signals in large cerebral veins. *Journal of Cerebral Blood Flow and Metabolism: Official Journal of the International Society of Cerebral Blood Flow and Metabolism*, *31*(2), 401–412.

Bianciardi, M., Fukunaga, M., van Gelderen, P., Horovitz, S. G., de Zwart, J. A., Shmueli, K., & Duyn, J. H. (2009). Sources of functional magnetic resonance imaging signal fluctuations in the human brain at rest: A 7 T study. *Magnetic Resonance Imaging*, *27*(8), 1019–1029.

Boorman, L., Kennerley, A. J., Johnston, D., Jones, M., Zheng, Y., Redgrave, P., & Berwick, J. (2010). Negative blood oxygen level dependence in the rat: A model for investigating the role of suppression in neurovascular coupling. *The Journal of Neuroscience: The Official Journal of the Society for Neuroscience*, *30*(12), 4285–4294.

Brasted, P. J., & Wise, S. P. (2004). Comparison of learning-related neuronal activity in the dorsal premotor cortex and striatum. *European Journal of Neuroscience*, *19*(3), 721–740.

Bright, M. G., Bianciardi, M., de Zwart, J. A., Murphy, K., & Duyn, J. H. (2014). Early anti-correlated BOLD signal changes of physiologic origin. *Neuroimage*, *87*, 287–296.

Chumbley, J., Worsley, K., Flandin, G., & Friston, K. (2010). Topological FDR for neuroimaging. *Neuroimage*, *49*(4), 3057–3064.

Deiber, M. P., Passingham, R. E., Colebatch, J. G., Friston, K. J., Nixon, P. D., & Frackowiak, R. S. (1991). Cortical areas and the selection of movement: A study with positron emission tomography. *Experimental Brain Research*, *84*(2), 393–402.

Downar, J., Crawley, A. P., Mikulis, D. J., & Davis, K. D. (2000). A multimodal cortical network for the detection of changes in the sensory environment. *Nature Neuroscience*, *3*(3), 277–283.

Frangi, A. F., Niessen, W. J., Vincken, K. L., & Viergever, M. A. (1998). Multiscale vessel enhancement filtering. *Medical Image Computing and Computer-Assisted Intervention - Miccai'98*, *1496*, 130–137.

Gonzalez-Castillo, J., Hoy, C. W., Handwerker, D. A., Roopchansingh, V., Inati, S. J., Saad, Z. S., … Bandettini, P. A. (2015). Task dependence, tissue specificity, and spatial distribution of widespread activations in large single-subject functional MRI datasets at 7T. *Cerebral Cortex (New York, N.Y.: 1991)*, *25*(12), 4667–4677.

Graziano, M. S., Yap, G. S., & Gross, C. G. (1994). Coding of visual space by premotor neurons. *Science (New York, N.Y.)*, *266*(5187), 1054–1057.

Greicius, M. D., Krasnow, B., Reiss, A. L., & Menon, V. (2003). Functional connectivity in the resting brain: A network analysis of the default mode hypothesis. *Proceedings of the National Academy of Sciences of the United States of America*, *100*(1), 253–258.

Greve, D. N., & Fischl, B. (2009). Accurate and robust brain image alignment using boundary-based registration. *Neuroimage*, *48*(1), 63–72.

Griffanti, L., Salimi-Khorshidi, G., Beckmann, C. F., Auerbach, E. J., Douaud, G., Sexton, C. E., … Mackay, C. E. (2014). ICA-based artefact removal and accelerated fMRI acquisition for improved resting state network imaging. *Neuroimage*, *95*, 232–247.

Guyton, A. C., & Hall, J. E. (2006). *Textbook of medical physiology*. Philadelphia: Elsevier Saunders. xxxv, 1116. p. p.

Hagler, D. J., Jr., Saygin, A. P., & Sereno, M. I. (2006). Smoothing and cluster thresholding for cortical surface-based group analysis of fMRI data. *Neuroimage*, *33*(4), 1093–1103.

Hamzei, F., Dettmers, C., Rzanny, R., Liepert, J., Buchel, C., & Weiller, C. (2002). Reduction of excitability ("inhibition") in the ipsilateral primary motor cortex is mirrored by fMRI signal decreases. *Neuroimage*, *17*(1), 490–496.

Hillman, E. M. (2014). Coupling mechanism and significance of the BOLD signal: A status report. *Annual Review of Neuroscience*, *37*, 161–181.

Hlushchuk, Y., & Hari, R. (2006). Transient suppression of ipsilateral primary somatosensory cortex during tactile finger stimulation. *The Journal of Neuroscience: The Official Journal of the Society for Neuroscience*, *26*(21), 5819–5824.

Janz, C., Heinrich, S. P., Kornmayer, J., Bach, M., & Hennig, J. (2001). Coupling of neural activity and BOLD fMRI response: New insights by combination of fMRI and VEP experiments in transition from single events to continuous stimulation. *Magnetic Resonance in Medicine*, *46*(3), 482–486.

Jenkinson, M., Bannister, P., Brady, M., & Smith, S. (2002). Improved optimization for the robust and accurate linear registration and motion correction of brain images. *Neuroimage*, *17*(2), 825–841.

Jezzard, P., Matthews, P. M., & Smith, S. M. (2001). *Functional MRI: An introduction to methods*. Oxford; New York: Oxford University Press. xiii, 390. p. p.

Jorge, J., Figueiredo, P., van der Zwaag, W., & Marques, J. P. (2013). Signal fluctuations in fMRI data acquired with 2D-EPI and 3D-EPI at 7 Tesla. *Magnetic Resonance Imaging*, *31*(2), 212–220.

Kastrup, A., Baudewig, J., Schnaudigel, S., Huonker, R., Becker, L., Sohns, J. M., … Witte, O. W. (2008). Behavioral correlates of negative BOLD signal changes in the primary somatosensory cortex. *Neuroimage*, *41*(4), 1364–1371.

Kayser, C., Petkov, C. I., Augath, M., & Logothetis, N. K. (2007). Functional imaging reveals visual modulation of specific fields in auditory cortex. *The Journal of Neuroscience: The Official Journal of the Society for Neuroscience*, *27*(8), 1824–1835.

Kelly, R. E., Jr., Alexopoulos, G. S., Wang, Z., Gunning, F. M., Murphy, C. F., Morimoto, S. S., … Hoptman, M. J. (2010). Visual inspection of independent components: Defining a procedure for artifact removal from fMRI data. *Journal of Neuroscience Methods*, *189*(2), 233–245.

Klingner, C. M., Hasler, C., Brodoehl, S., & Witte, O. W. (2010). Dependence of the negative BOLD response on somatosensory stimulus intensity. *Neuroimage*, *53*(1), 189–195.

Klingner, C. M., Huonker, R., Flemming, S., Hasler, C., Brodoehl, S., Preul, C., … Witte, O. W. (2011). Functional deactivations: Multiple ipsilateral brain areas engaged in the processing of somatosensory information. *Human Brain Mapping*, *32*(1), 127–140.

Koopmans, P. J., Barth, M., & Norris, D. G. (2010). Layer-specific BOLD activation in human V1. *Human Brain Mapping*, *31*(9), 1297–1304.

Laurienti, P. J., Burdette, J. H., Wallace, M. T., Yen, Y. F., Field, A. S., & Stein, B. E. (2002). Deactivation of sensory-specific cortex by cross-modal stimuli. *Journal of Cognitive Neuroscience*, *14*(3), 420–429.

Lauritzen, M., Mathiesen, C., Schaefer, K., & Thomsen, K. J. (2012). Neuronal inhibition and excitation, and the dichotomic control of brain hemodynamic and oxygen responses. *Neuroimage*, *62*(2), 1040–1050.

Lee, T. W., Girolami, M., & Sejnowski, T. J. (1999). Independent component analysis using an extended infomax algorithm for mixed subgaussian and supergaussian sources. *Neural Computation*, *11*(2), 417–441.

Lin, P., Hasson, U., Jovicich, J., & Robinson, S. (2011). A neuronal basis for task-negative responses in the human brain. *Cerebral Cortex (New York, N.Y.: 1991)*, *21*(4), 821–830.

Lindquist, M. A., & Wager, T. D. (2007). Validity and power in hemodynamic response modeling: A comparison study and a new approach. *Human Brain Mapping*, *28*(8), 764–784.

Marques, J. P., Kober, T., Krueger, G., van der Zwaag, W., Van de Moortele, P. F., & Gruetter, R. (2010). MP2RAGE, a self bias-field corrected sequence for improved segmentation and T1-mapping at high field. *Neuroimage*, *49*(2), 1271–1281.

Mayer, J. S., Roebroeck, A., Maurer, K., & Linden, D. E. (2010). Specialization in the default mode: Task-induced brain deactivations dissociate between visual working memory and attention. *Human Brain Mapping*, *31*(1), 126–139.

Mayhew, S. D., Mullinger, K. J., Ostwald, D., Porcaro, C., Bowtell, R., Bagshaw, A. P., & Francis, S. T. (2016). Global signal modulation of single-trial fMRI response variability: Effect on positive vs negative BOLD response relationship. *Neuroimage*, *133*, 62–74.

Mayhew, S. D., Ostwald, D., Porcaro, C., & Bagshaw, A. P. (2013). Spontaneous EEG alpha oscillation interacts with positive and negative BOLD responses in the visual-auditory cortices and default-mode network. *Neuroimage*, *76*, 362–372.

Menon, R. S. (2002). Postacquisition suppression of large-vessel BOLD signals in high-resolution fMRI. *Magnetic Resonance in Medicine*, *47*(1), 1–9.

Mullinger, K. J., Mayhew, S. D., Bagshaw, A. P., Bowtell, R., & Francis, S. T. (2014). Evidence that the negative BOLD response is neuronal in origin: A simultaneous EEG-BOLD-CBF study in humans. *Neuroimage*, *94*, 263–274.

Mumford, J. A., Poline, J. B., & Poldrack, R. A. (2015). Orthogonalization of regressors in FMRI models. *PLoS One*, *10*(4), e0126255.

Pasley, B. N., Inglis, B. A., & Freeman, R. D. (2007). Analysis of oxygen metabolism implies a neural origin for the negative BOLD response in human visual cortex. *Neuroimage*, *36*(2), 269–276.

Salimi-Khorshidi, G., Douaud, G., Beckmann, C. F., Glasser, M. F., Griffanti, L., & Smith, S. M. (2014). Automatic denoising of functional MRI data: Combining independent component analysis and hierarchical fusion of classifiers. *Neuroimage*, *90*, 449–468.

Setsompop, K., Gagoski, B. A., Polimeni, J. R., Witzel, T., Wedeen, V. J., & Wald, L. L. (2012). Blipped-controlled aliasing in parallel imaging for simultaneous multislice echo planar imaging with reduced g-factor penalty. *Magnetic Resonance in Medicine*, *67*(5), 1210–1224.

Shmuel, A., Augath, M., Oeltermann, A., & Logothetis, N. K. (2006). Negative functional MRI response correlates with decreases in neuronal activity in monkey visual area V1. *Nature Neuroscience*, *9*(4), 569–577.

Shmuel, A., Yacoub, E., Chaimow, D., Logothetis, N. K., & Ugurbil, K. (2007). Spatio-temporal point-spread function of fMRI signal in human gray matter at 7 Tesla. *Neuroimage*, *35*(2), 539–552.

Shmuel, A., Yacoub, E., Pfeuffer, J., Van de Moortele, P. F., Adriany, G., Hu, X., & Ugurbil, K. (2002). Sustained negative BOLD, blood flow and oxygen consumption response and its coupling to the positive response in the human brain. *Neuron*, *36*(6), 1195–1210.

Smith, A. T., Williams, A. L., & Singh, K. D. (2004). Negative BOLD in the visual cortex: Evidence against blood stealing. *Human Brain Mapping*, *21*(4), 213–220.

Smith, S. M. (2002). Fast robust automated brain extraction. *Human Brain Mapping*, *17*(3), 143–155.

Smith, S. M., Beckmann, C. F., Andersson, J., Auerbach, E. J., Bijsterbosch, J., Douaud, G., ... Harms, M. P. (2013). Resting-state fMRI in the Human Connectome Project. *Neuroimage*, *80*, 144–168.

Stefanovic, B., Warnking, J. M., & Pike, G. B. (2004). Hemodynamic and metabolic responses to neuronal inhibition. *Neuroimage*, *22*(2), 771–778.

Thomas, B. P., Liu, P., Park, D. C., van Osch, M. J., & Lu, H. (2014). Cerebrovascular reactivity in the brain white matter: Magnitude, temporal characteristics, and age effects. *Journal of Cerebral Blood Flow and Metabolism: Official Journal of the International Society of Cerebral Blood Flow and Metabolism*, *34*(2), 242–247.

Turner, R. (2002). How much cortex can a vein drain? Downstream dilution of activation-related cerebral blood oxygenation changes. *Neuroimage*, *16*(4), 1062–1067.

Vafaee, M. S., & Gjedde, A. (2004). Spatially dissociated flow-metabolism coupling in brain activation. *Neuroimage*, *21*(2), 507–515.

van der Zwaag, W., Francis, S., Head, K., Peters, A., Gowland, P., Morris, P., & Bowtell, R. (2009a). fMRI at 1.5, 3 and 7 T: Characterising BOLD signal changes. *Neuroimage*, *47*(4), 1425–1434.

van der Zwaag, W., Marques, J. P., Hergt, M., & Gruetter, R. (2009b). Investigation of high-resolution functional magnetic resonance imaging by means of surface and array radiofrequency coils at 7 T. *Magnetic Resonance Imaging*, *27*(8), 1011–1018.

Wade, A. R. (2002). The negative BOLD signal unmasked. *Neuron*, *36*(6), 993–995.

Worsley, K. J., & Friston, K. J. (1995). Analysis of fMRI time-series revisited–again. *Neuroimage*, *2*(3), 173–181.

Yacoub, E., Shmuel, A., Pfeuffer, J., Van De Moortele, P. F., Adriany, G., Andersen, P., ... Hu, X. (2001). Imaging brain function in humans at 7 Tesla. *Magnetic Resonance in Medicine*, *45*(4), 588–594.

Zhang, Y., Brady, M., & Smith, S. (2001). Segmentation of brain MR images through a hidden Markov random field model and the expectation-maximization algorithm. *IEEE Transactions on Medical Imaging*, *20*(1), 45–57.

SUPPORTING INFORMATION

Additional Supporting Information may be found online in the supporting information tab for this article.

How to cite this article: Jorge J, Figueiredo P, Gruetter R, van der Zwaag W. Mapping and characterization of positive and negative BOLD responses to visual stimulation in multiple brain regions at 7T. *Hum Brain Mapp*. 2018;39:2426–2441. https://doi.org/10.1002/hbm.24012